Published in final edited form as:

Mol Cancer Res. 2017 September ; 15(9): 1138–1152. doi:10.1158/1541-7786.MCR-17-0003.

Infiltrating Myeloid Cells Exert Pro-Tumorigenic Actions via Neutrophil Elastase

Irina Lerman[1], **Maria de la Luz Garcia-Hernandez**[2], **Javier Rangel-Moreno**[3], **Luis Chiriboga**[4], **Chunliu Pan**[5], **Kent L. Nastiuk**[5], **John J. Krolewski**[5], **Aritro Sen**[1], and **Stephen R. Hammes**[1]

[1]Department of Medicine, Division of Endocrinology and Metabolism, University of Rochester Medical Center, Rochester, NY

[2]Department of Medicine, Aab Cardiovascular Research Institute, University of Rochester Medical Center, Rochester, NY

[3]Department of Medicine, Division of Allergy/Immunology and Rheumatology, University of Rochester Medical Center, Rochester, NY

[4]Department of Pathology, NYU Langone Medical Center, New York, NY

[5]Department of Cancer Genetics, Roswell Park Cancer Institute, Buffalo, NY

Abstract

Tissue infiltration and elevated peripheral circulation of granulocytic myeloid-derived cells is associated with poor outcomes in prostate cancer (PCa) and other malignancies. Although myeloid-derived cells have the ability to suppress T-cell function, little is known about the direct impact of these innate cells on prostate tumor growth. Here it is reported that granulocytic myeloid-derived suppressor cells (MDSCs) are the predominant tumor infiltrating cells in PCa xenografts established in athymic nude mice. MDSCs significantly increased in number in the peripheral circulation as a function of xenograft growth and were successfully depleted in vivo by Gr-1 antibody treatment. Importantly, MDSC depletion significantly decreased xenograft growth. We hypothesized that granulocytic MDSCs might exert their pro-tumorigenic actions in part through neutrophil elastase (ELA2/NE), a serine protease released upon granulocyte activation. Indeed, it was determined that NE is expressed by infiltrating immune cells and is enzymatically active in PCa xenografts and in prostate tumors of prostate-specific Pten-null mice. Importantly, treatment with sivelestat, a small-molecule inhibitor specific for NE, significantly decreased xenograft growth, recapitulating the phenotype of Gr-1 MDSC depletion. Mechanistically, NE activated mitogen-activated protein kinase (MAPK) signaling and induced MAPK-dependent transcription of the proliferative gene cFOS in PCa cells. Functionally, NE stimulated proliferation, migration, and invasion of PCa cells in vitro. Immunohistochemistry (IHC) on human PCa clinical biopsies revealed co-expression of NE and infiltrating CD33+ MDSCs.

Corresponding Author: Stephen R. Hammes, MD, PhD, Department of Medicine, Division of Endocrinology and Metabolism, University of Rochester School of Medicine, 601 Elmwood Ave., Rochester, NY 14642. Phone: 585-276-4995; Fax: 585-273-1288; stephen_hammes@urmc.rochester.edu.

Keywords

Prostate cancer; myeloid derived suppressor cells (MDSC); neutrophil elastase

Introduction

Inflammation is important to consider when studying prostate cancer microenvironment, for both prognostic and therapeutic purposes (1). Chronic inflammation in initially benign tissue confers an increased risk of subsequent cancer diagnosis, and elevated pro-inflammatory cytokines are associated with shorter times to castration resistance and lower overall survival (2–4). Establishing peripheral blood biomarkers of inflammation as prognostic indicators in cancer has become particularly attractive. For instance, elevated indexes of systemic inflammation such as the Neutrophil to Lymphocyte ratio (NLR) and the modified Glasgow Prognostic Score consistently predict decreased survival in localized and advanced prostate cancer (5, 6). Interestingly, patients who convert from high NLR to low NLR over the course of treatment have significantly improved survival compared to those who maintain high NLR status (7). In fact, granulocytic infiltrates are predictive of poor survival in nearly all examined human malignancies, as demonstrated by a large-scale transcriptomic analysis of ~18,000 human tumors (8). In accordance with this finding, gene expression profiling of peripheral blood mononuclear cells (PBMCs) isolated from advanced castration-resistant prostate cancer patients reveals that the majority of up-regulated genes conferring poor prognosis are associated with gene signatures of granulocytes (9, 10).

One of the most significantly up-regulated genes identified in these studies is *ELANE*, which encodes neutrophil elastase (NE) (9, 10). The pro-tumorigenic role of NE has been established in lung, breast, and colon cancers, among others (11–14). Global deletion of NE in genetic mouse models of breast and lung cancer notably reduces the number and size of tumors (11, 12, 14). NE may contribute to tumor growth by directly increasing proliferation, migration, and invasion of cancer cells or by inducing angiogenesis within the microenvironment; it may also contribute to tumorigenesis by inactivating tumor suppressors, thereby disinhibiting growth (11, 15–18). Moreover, NE is one of the main mediators of neutrophil extracellular trap (NET) formation (19). NETs are externalized protease-laden DNA fibers released upon neutrophil activation in response to infection or cancer burden (20). NETs play an important role in cancer pathology, promoting primary tumor growth and development of a metastatic niche (21–23). In the context of prostate cancer, tumor-derived cytokines like IL8 have been shown to attract myeloid-derived suppressor cells (MDSCs) and elicit extrusion of NETs within the tumor microenvironment (24). Beyond this, the functional role of NETs and their associated proteases such as NE has not been addressed in prostate cancer.

In humans, distinguishing neutrophils from granulocytic MDSCs is challenging (25). Like neutrophils, these granulocytic myeloid-derived cells expand in the periphery of tumor bearing mice and patients with a variety of cancers, including prostate cancer (4, 26–28). In fact, increased tumor infiltration of CD33+ MDSCs is correlated with human prostate cancer progression and diminished overall survival (26, 29). Not only are MDSCs markers of

aggressive cancer, they also appear to actively promote tumor progression. Studies demonstrate a functional role for MDSCs in various cancers, as their depletion with Gr-1 antibodies or other methods generally improves outcomes in mouse models of cancer (25). In prostate cancer, MDSC depletion with Gr-1 antibodies or interruption of lesion recruitment with CXCR2 and CSF1R inhibitors reduces tumor size and slows disease progression in probasin-driven *Pten*-null prostate cancer mouse models (26, 29, 30). Dissection of the pro-tumoral mechanisms of MDSCs has predominantly focused on their immunosuppressive effects on T-cell function (thought to derive primarily from monocytic MDSCs) rather than their direct effects on cancer cell growth, migration, and invasion (28). However, transcriptomic analysis of MDSCs isolated from tumor-bearing animals reveals significant enrichment in NE compared to non-tumor controls (31, 32). Given the aforementioned pro-tumorigenic potential of NE, these observations suggest a potentially important role for granulocytic MDSCs, neutrophils, and NE in regulating tumor progression.

Here we investigated the role of granulocytic MDSCs and NE in facilitating prostate cancer xenograft growth in athymic mice. Our findings demonstrate that NE facilitates the pro-tumor role of granulocytic MDSCs in the absence of T-cell suppression. Our studies further demonstrate that NE can directly stimulate human prostate cancer cell proliferation, migration and invasion *in-vitro*, in part by activating the MAPK pathway. Together, our results provide a rationale for exploiting elevated NLR and granulocytic MDSCs levels, as well as NE expression, in prostate cancer patients not only as biomarkers of disease burden, but also as potential targets of therapeutic intervention.

Materials and Methods

Cell Culture

PC3 (authenticated by ATCC upon purchase) and C4-2 (from Ganesh Raj, UTSW) cells were cultured in RPMI-1640 media (Gibco) with 10% fetal bovine serum (FBS; Seradigm) and 1% penicillin-streptomycin (P-S; Gibco). Cells were maintained at 37°C, 95% air, and 5% CO_2. Experiments were performed with cells below passage 25. Mycoplasm testing was not performed.

Animal studies

Experiments were performed in accordance with the guidelines for the Care and Use of Laboratory Animals and approved by the University Committee on Animal Resources at the University of Rochester. For Gr-1 depletion, 6–8 week old male athymic nude mice (J:NU 007850, Jackson Laboratories) were subcutaneously injected with 3×10^6 PC3 cells in 0.1mL PBS. When tumors became palpable (approximately three weeks), mice were randomized into Gr-1 depletion and isotype control groups. Gr-1 depletion was performed by intraperitoneal (IP) injection of 200μg rat anti-mouse Ly6G/Ly6C (Gr-1) antibody (clone RB6-8C5, catalog#BE0075, BioXCell) three times/week. Isotype controls received 200μg rat IgG2b (clone LTF-2, catalog#BE0090, BioXCell) via IP injection three times/week. Xenograft size was calculated using the formula: $LxW^2x0.5$. For NE inhibition, 6–8 week old male athymic nude mice were subcutaneously injected with 3×10^6 PC3 cells in 0.1mL

PBS or 5×10^6 C4-2 cells in 0.1mL of a 1:1 mixture of Matrigel (Corning) and PBS. When tumors became palpable (approximately three weeks for PC3, four weeks for C4-2), mice were randomized into sivelestat or vehicle groups. Sivelestat (Tocris) was administered via IP injection at 5mg/kg (in 4% DMSO 0.1mL PBS) daily, and 4% DMSO 0.1mL PBS was used as vehicle control.

Experimental work with the prostate-specific *Pten*-null mouse model was approved by the Roswell Park IACUC. Tumorigenesis in the PbCre4/Pten^{fl} model is driven by Pten loss specific to the prostatic epithelium (30), a very common alteration in human prostate cancer. This deletion was carried out in C57BL/6N mice. Tumors are histologically characterized primarily as high-grade prostatic intraepithelial neoplasia (HG-PIN, sometimes called mPIN3/4). Tumor volume was monitored using our 3D ultrasound imaging protocol (33) to only examine NE activity in mice bearing tumors of 300–500 mm^3. For the *ex-vivo* fluorescent imaging, the entire GU bloc was dissected out, the bladder was removed, and the prostate was visually verified. The region of interest that was quantified included the entire prostate tumor plus normal tissue (ventral, dorsal, lateral, anterior lobes). The tumor volume (300–500mm^3) made up ~80%-90% of the total volume of the tissue examined in the region of interest.

Flow cytometry

Blood was collected from retro-orbital sinuses at indicated times to monitor efficacy of Gr-1 depletion. White blood cells were separated with 1-Step Polymorphs solution (Accurate Chemical). Residual red blood cells were lysed with ACK buffer (150mM NH_4Cl, 10mM $KHCO_3$, 1mM Na_2EDTA, pH 7.2), and neutralized with FACS media (2% FBS, 2.5mM EDTA in PBS). Live cells were counted on a hemocytometer based on trypan blue exclusion. Cells were blocked with 50μg/mL rat anti-mouse CD16/CD32 Fc (catalog#BE008, BioXCell) and stained with rat anti-mouse CD11b-APC/Cy7 (1:100, catalog#101226, Biolegend), rat anti-mouse Ly6C-PE (1:100, catalog#12-5932-82, eBioscience), rat-anti-mouse Ly6G-Biotin (1:100, catalog#127604, Biolegend). Streptavidin-FITC (1:200, catalog#554060, BD Biosciences) was used to reveal biotinylated antibody. All dilutions and washes were carried out in FACS media. Propidium iodide (Sigma-Aldrich) used at 0.1μg/mL to exclude dead cells from analysis. Cells were collected on a LSRII flow cytometer (BD Biosciences) and analyzed with FlowJo 10.1r7 software. Gr-1 depletion in peripheral blood was verified using an automated 5-part differential cell counter (VetScan HM5; Abaxis). For flow cytometry on xenografts, xenografts were digested in 0.1% dispase (Worthington) in FACS media for 30 minutes at 37°C and mechanically dissociated. The following primary antibodies were used: rat-anti-mouse CD45-APC/Cy7 (1:50, catalog#103115, Biolegend), rat-anti-mouse CD11b-APC (1:100, catalog#101212, Biolegend), rat anti-mouse Ly6C-PE, rat-anti-mouse Ly6G-Biotin.

Immunohistochemistry

5μm xenograft sections were de-paraffinized with xylene and rehydrated in graded ethanol/water. Heat-mediated antigen retrieval was performed in 0.01M Citrate pH 6 at 95°C. Rabbit anti-mouse/human neutrophil elastase (catalog#ab68672, Abcam) was diluted 1:200 in antibody diluent (Thermo Scientific) and incubated overnight at 4°C. Biotinylated goat anti-

rabbit IgG (cat#BA-1000, Vector Laboratories) was diluted 1:200 in blocking serum (1.5% normal goat serum in PBS), and immunoreactivity detected using the Vectastain Elite ABC and DAB peroxidase substrate kits (Vector Laboratories). Immunohistochemistry for NE and CD33 on human prostate tissue microarrays was performed on an automated platform (Ventana Discovery XT) using rabbit anti-mouse/human neutrophil elastase (1:75) and mouse anti-human CD33 (1:50, catalog#133M-15, Sigma-Aldrich) primary antibodies. Primary antibodies were detected with either anti-mouse/rabbit HRP-DAB or anti-mouse/rabbit HRP-FITC/Rhodamine. Chromogenic sections were counterstained with hematoxylin and mounted using Cytoseal 60 (Thermo Scientific).

Immunofluorescence

Paraffin-embedded sections were processed as described above. Antigen unmasking was performed using Target Retrieval Solution 10× (Dako). Primary antibodies used were: biotin-conjugated rat anti-mouse Ly6B.2 (1:50, catalog#MCA771G, BioRad), goat anti-mouse PCNA (1:50, catalog#sc-9857, Santa Cruz), and rabbit anti-human ki67 (1:200, catalog#ab66155, Abcam). Primary antibodies were detected with Streptavidin Alex Fluor 488 (1:200, catalog#511223, Invitrogen), donkey anti-rat Alexa Fluor 488 (1:200, catalog#A21208, Invitrogen), donkey anti-goat Alexa Fluor 568 (1:200, catalog#A11057, LifeTech), and goat anti-rabbit Texas Red (1:200, catalog#TI-1000, Vector Laboratories). Whole-mount immunofluorescence for xenograft infiltrating Gr-1 cells was performed using rat anti-mouse Gr-1 antibody conjugated to Alexa Fluor 488 (catalog#108417, Biolegend), as previously described (34). In short, a small piece (~15mg) of tumor was stained and placed between microscopy grade coverslips using a home-built device prior to imaging. Therefore, it provides a flattened representation of the immune cells within the entire piece of tumor.

NE imaging

Two weeks prior to xenograft imaging, mice were placed on an alfalfa-free diet, 2016 Teklad global 16% protein (Envigo). Mice received 4 nmols of Neutrophil Elastase 680 FAST (Perkin Elmer) probe in 0.1mL PBS via tail-vein injection and imaged 16 hours later using the in-vivo imaging system IVIS Spectrum (Perkin Elmer). Images were processed using Living Image 3.2 software (Perkin Elmer). Activity measurements were performed on excised tumors using fluorescent microscopy and intensity was analyzed using ImageJ v1.48 software.

Westerns

PC3 and C4-2 cells were plated at 2×10^5 cells per well in 6-well plates in complete media (10% FBS, 1% P-S, RPMI-1640). After 48 hours, cells were placed in serum-free, 1% P-S, RPMI-1640 for 16 hours and stimulated with indicated concentrations of NE (cat#IHNE, Innovative Research) for 15 minutes. For NE inhibitor studies, sivelestat was incubated directly with NE at indicated concentrations for 30 minutes prior to addition to the cells. Cells were lysed in RIPA (Pierce) supplemented with 1× Halt protease and phosphatase inhibitor cocktail (Thermo Scientific). Samples were processed for gel electrophoresis and Western blotted with rabbit anti-phospho-Erk1/2 (1:1000, catalog#9101, Cell Signaling) and

rabbit anti-total-Erk1/2 (1:1000, catalog#9102, Cell Signaling) as previously described (35). Band densitometry was performed using ImageJ v1.48 software.

Quantitative PCR

C4-2 cells were plated at 2×10^5 cells per well in 6-well plates and serum starved for 16 hours before stimulation with 2.5μg/mL NE for 6 hours. Pre-treatments were performed as indicated with 2μM of sivelestat or 50nM of PD0325901 (Selleckchem). RNA was extracted using the E.Z.N.A. kit (Omega). Quantitative PCR (qPCR) was performed using the TaqMan RNA-to-Ct™ 1-Step Kit (Applied Biosystems) and TaqMan primers (Applied Biosystems) for human *FOS* (Hs00170630_m1) and *GAPDH* (Hs03929097_g1). Human *FOS* mRNA was normalized to human *GAPDH* using the ΔΔCt method. For determination of NE expression in xenografts, RNA was extracted using the E.Z.N.A. kit, and qPCR performed using TaqMan primers species-specific for human *ELANE* (Hs00975994_g1), human *GAPDH* (Hs03929097_g1), mouse *Elane* (Mm00469310_m1), and mouse *Gapdh* (Mm99999915_g1). *ELANE* and *Elane* mRNA levels were normalized to *GAPDH* and *Gapdh*, respectively, using the ΔΔCt method.

Proliferation assay

C4-2 cells were plated at 3×10^4 cells per well in 24-well plates in complete media and then in 1% FBS, 1% P-S, RPMI-1640 for 16 hours before stimulation with 2.5μg/mL NE for 24 hours. Pre-treatments were performed as indicated with 5μM of sivelestat or 50nM PD0325901. Proliferation was assessed using the BrdU Cell Proliferation Assay Kit (Cell Signaling) with slight modification. Briefly, 1× 5-bromo-2'-deoxyuridine (BrdU) was added directly to cell media and incubated for 2 hours at 37°C. Cells were fixed in 4% paraformaldehyde in PBS (Affymetrix) and DNA was denatured with 2N HCl. Cells were blocked with 1.5% normal horse serum (Vector Laboratories) in 0.2% Triton X-100 (Fisher BioReagents) PBS. Remaining steps were performed according to manufacturer's instructions.

Migration assay

C4-2 and PC3 cells (1×10^6) were plated in a 10cm dish in complete media and serum starved for 20 hours. Cells were seeded at a density of 1.5×10^5 cells per well in serum-free media into the upper chambers of 8μm-pore 24-well transwell permeable supports (Corning) and stimulated with 2.5μg/mL NE. Pre-treatments were performed as indicated with 5μM of sivelestat or 50nM PD0325901. Complete media was used in the bottom chamber, and cells were allowed to migrate for 24 hours. Unmigrated cells were removed from the inner side of the upper chamber. Migrated cells were fixed in 4% PFA in PBS and stained with 0.2% crystal violet (Sigma-Aldrich). Membranes were washed with H_2O and counted in 5 random fields. Number of migrated cells was quantified with ImageJ v1.48 software.

Invasion assay

C4-2 and PC3 cells were plated as described for the migration assay and seeded at a density of 2×10^5 cells per well in serum-free media into the upper chamber of BioCoat Matrigel

8μm-pore 24-well transwell permeable supports (Corning). Treatments, processing, and analysis were carried out as described for the migration assay.

Statistical analysis

Data are presented as mean ± standard error of the mean (SEM). Comparison between two groups was performed using two-tailed t-test, unless otherwise indicated. Comparison between more than two groups was performed using one-way ANOVA with appropriate post-hoc testing. All statistical analyses were performed using GraphPad Prism 7.0 software, and significance defined as $p<0.05$.

Results

Circulating granulocytic MDSCs expand during human prostate cancer xenograft growth

To study the role of myeloid-derived cells in prostate cancer growth, we used immunodeficient athymic nude mice lacking functional adaptive immunity. The immunologic parameters of the specific athymic mouse strain (J:NU 007850) used in our experiments have been thoroughly characterized by the Jackson Laboratory. Since T-cells comprise on average only 0.09% of all immune cells in these male athymic mice, we were able to essentially eliminate potential contributions of MDSCs to T-cell suppression and focus on their direct effects on tumor cell growth and survival.

We established subcutaneous prostate cancer xenografts using the most aggressive human cell line that we could find – PC3 cells. We allowed tumors to grow for approximately three weeks. We subsequently randomized the mice into two treatment groups: MDSC-depletion using Gr-1 antibody and control using IgG isotype antibody. On day 5 and 27 after treatment initiation, we assessed the number of circulating myeloid cells in peripheral blood by flow cytometry using CD11b, Ly6G, and Ly6C surface expression. Gating on CD11b, we observed that the granulocytic MDSC (Ly6G+/Ly6C+) population significantly expanded in the isotype-control treated mice as a function of tumor growth (Fig 1A, left). Accordingly, quantification of the Ly6G+/Ly6C+ population in peripheral blood revealed a doubling on day 27 compared to day 5 in the isotype-control group (Fig 1B). This Ly6G+/Ly6C+ population was significantly reduced with Gr-1 antibody treatment as early as day 5 and remained low on day 27 (Fig 1A & B), indicating successful depletion throughout treatment. Because Gr-1 antibody potentially blocks the epitope recognized by anti-Ly6G, we confirmed our flow cytometry results using automated cell counting for polymorphonuclear (PMN) cells as well as manual verification on blood smears (Fig 1C & D).

We next assessed tumor infiltrating immune cells in naïve, untreated PC3 tumors. Using whole-mount immunofluorescence for Gr-1, we observed MDSCs heterogenously infiltrating the PC3 tumor parenchyma (Fig 1E), confirming their abundance within the microenvironment. Dispersal of tumors followed by flow cytometry gated on CD45, CD11b, Ly6G, and Ly6C surface expression revealed that the majority of immune cells within prostate cancer tumors were CD11b+ myeloid cells (Fig 1F). Furthermore, most of these myeloid cells were granulocytic rather than monocytic (Fig 1G), indicating that granulocytic myeloid cells are the predominant innate cell population in our prostate cancer model.

Depletion of MDSCs suppresses human prostate cancer xenograft growth

We next evaluated the effect of Gr-1 antibody-mediated MDSC depletion within PC3 tumors using flow cytometry. Again, we observed a large population of Ly6G+/Ly6C+ granulocytic MDSCs in the isotype control tumors that was eliminated by Gr-1 antibody treatment at day 27 (Fig 2A & B). Given that anti-Gr-1 can potentially block Ly6G and Ly6C epitopes, we decided to use an antibody against Ly6B2 alloantigen to detect tumor infiltrating myeloid cells. Immunofluorescence staining of tumor sections showed a significant reduction in Ly6B+ cells in the Gr-1 antibody mice compared to isotype control, confirming depletion was efficient in the target tissue (Fig 2C & D). Importantly, depletion of MDSCs significantly reduced xenograft growth almost immediately and for several weeks, with a significant diminution of final tumor weight (Fig 2E & F). By flow cytometry, immune cells (CD45+) comprised on average 7.14% (0.89% SEM) of the final isotype control tumors and 4.01% (0.98% SEM) of the final Gr-1 depleted tumors ($p = 0.033$). Immune infiltrate depletion therefore would account for only a very small change in tumor volume, whereas we observed ~50% overall tumor size reduction; thus, the tumor mass was smaller primarily due to fewer tumor cells. Accordingly, we observed a reduction in proliferative Ki67 staining in the Gr-1 depleted tumors compared to isotype controls (Supplementary Fig 1 A & B). These results indicate that peripheral expansion and local infiltration of MDSCs have a pro-tumor effect even in the absence of adaptive immunity suppression.

Infiltrating immune cells produce active neutrophil elastase in the tumor microenvironment

Given that granulocytic MDSCs and neutrophils produce copious amounts of NE, and because NE is implicated in tumor growth in other cancers, we assessed whether NE was present and active in mouse models of prostate cancer using a bio-activatable optical probe consisting of two fluorophores linked to a peptide substrate specific to NE. The fluorophores are quenched in the intact probe but emit fluorescence upon cleavage. PC3 and C4-2 human prostate cancer xenografts demonstrated significant *in-vivo* (Fig 3A & B) signals, indicating that NE is highly active within these tumors. Immunohistochemistry for NE confirmed its expression in PC3 xenografts (Fig 3C, high power image in Supplementary Fig 2). Notably, human *NE* mRNA was not expressed by PC3 or C4-2 cells in culture (data not shown), nor was human *NE* mRNA expressed in PC3 or C4-2 xenografts (Fig 3D & E) using human specific qPCR primers. In contrast mouse *NE* was detected in PC3 and C4-2 xenografts using mouse specific qPCR primers (Fig 3D & E), supporting its origin exclusively from mouse-derived infiltrating immune cells.

Furthermore, we evaluated NE activity *ex-vivo* in tumors isolated from the *Pten*-null prostate cancer mouse model. Importantly, these mice have an intact immune system (30). As seen in the xenograft models in athymic mice, NE activity was significantly up-regulated in *Pten*-null prostate tumors compared to strain-matched normal prostates (Fig 3F & G), supporting a potential contribution to tumor growth in both immune-deficient and immune-competent mouse models of prostate cancer. We next assessed infiltrating immune cells in the *Pten*-null prostate tumors and again observed a significant infiltration of Ly6B+ granulocytic MDSCs, which were practically undetectable in normal prostates (Fig 3I). Moreover, the *Pten*-null prostate tumors were proliferative, demonstrated by epithelial positivity for proliferating cell nuclear antigen (PCNA), whereas the normal prostates were quiescent (Fig 3I). Notably, the

number of circulating granulocytic MDSCs was also elevated in *Pten*-null mice relative to wild-type mice (Fig 3H).

Inhibition of neutrophil elastase activity suppresses human prostate cancer xenograft growth

Since NE promotes tumor growth in mouse models of breast, lung, and colon cancer, we next evaluated its role in our prostate cancer xenografts. Using a similar experimental approach as the depletion experiment, we established subcutaneous PC3 xenografts and grew them to 100mm^3, at which point we randomized mice into sivelestat (specific NE inhibitor) and vehicle treatment groups. Sivelestat significantly reduced xenograft growth (Fig 4A) and final tumor weight (Fig 4B), recapitulating the effect of Gr-1 MDSC depletion. *Ex-vivo* quantification of tumor fluorescence after injection of the NE specific optical probe was significantly diminished with sivelestat treatment (Fig 4C & D), demonstrating effective inhibition in the target tissue.

To demonstrate that modulation of NE enzymatic activity was applicable to a different human prostate cancer cell line, and since we had observed NE activity in C4-2 xenografts (Fig 3B), we treated C4-2 xenograft bearing mice with sivelestat. We found that sivelestat significantly reduced xenograft growth (Fig 4E) and final tumor weight (Fig 4F). We similarly verified NE inhibition in C4-2 tumors, as *ex-vivo* quantification of tumor fluorescence was significantly diminished with sivelestat treatment (Fig 4G & H). Our findings demonstrate NE activity as a potential therapeutic target, since inhibition suppresses xenograft growth of two human prostate cancer cell lines.

Neutrophil elastase promotes proliferation, migration, and invasion of prostate cancer cell lines

Next we sought to determine the mechanism by which NE promotes prostate cancer progression. NE can activate mitogen-activated protein kinase (MAPK) signaling in some cell types, so we examined its ability to induce ERK1/2 phosphorylation in prostate cancer cells *in-vitro*. Indeed, we observed a dose-dependent induction of ERK1/2 phosphorylation in PC3 cells, with maximal induction occurring at a dose of 2.5μg/mL (Fig 5A). All subsequent experiments were performed using this NE dose. Time course experiments revealed maximal induction at 15 minutes of treatment with NE (not shown), suggesting rapid activation of the MAPK pathway. NE mediated ERK1/2 activation was dependent on enzymatic activity, as sivelestat blocked ERK1/2 phosphorylation (Fig 5B). All subsequent *in-vitro* experiments involving sivelestat were performed with the lowest dose (2μM) tested. NE-induced ERK1/2 phosphorylation was significant and abrogated by pre-treatment with sivelestat in both PC3 (Fig 5C) and C4-2 cells (Fig 5D), quantified by Western blot band densitometry (graphs below).

Next we assessed the functional outcome of NE-induced MAPK activation. An important downstream effect of ERK1/2 phosphorylation is induction of gene transcription. c*FOS* is an ERK1/2 dependent proliferative gene, so we measured its transcription in response to NE. NE significantly up-regulated *cFOS* mRNA expression (Fig 5E) in C4-2 cells, and this was blocked by pre-treatment with sivelestat or MEK-inhibitor PD0325901 (Fig 5E). NE also

significantly stimulated C4-2 cell proliferation, determined by BrdU incorporation, which was blocked by pre-treatment with sivelestat (Fig 5F). Notably, treatment with sivelestat alone did not significantly reduce proliferation (Fig 5F), suggesting that sivelestat does not act directly on the cells. Conversely, treatment with PD0325901 alone significantly reduced proliferation (Fig 5F), confirming MAPK as an important proliferative pathway in these cells. NE was unable to induce proliferation in the presence of PD0325901 (Fig 5F), suggesting that NE-induced C4-2 cell proliferation is dependent on MAPK signaling.

Next we assessed the effects of NE on the migratory and invasive potential of C4-2 and PC3 prostate cancer cells using transwell assays. NE significantly increased migration (Fig 6A & C for C4-2, Fig 6E for PC3) and invasion (Fig 6B & D for C4-2, Fig 6F for PC3), and both were blocked by sivelestat. PD0325901 was unable to inhibit NE-induced migration (Fig 6C & E), indicating that this is likely a MAPK-independent process. However, PD0325901 appeared to mitigate NE-induced invasion (Fig 6D & F), suggesting that, unlike migration, this process may have a different, potentially MAPK-dependent, mechanism.

CD33+ MDSCs are a source of neutrophil elastase in human prostate cancer

We next looked for expression of CD33+ MDSCs and NE in human prostate cancer samples using immunohistochemistry. We detected weak positivity of NE in the stroma, along with strong positivity in infiltrating and intra-luminal cells with granulocytic morphology (Fig 7A). Furthermore, we observed strong positivity in corpora amylacea or prostatic concretions (Fig 7A, arrowhead), in agreement with previous work identifying granulocyte-derived factors in these structures (36). Since activated immune cells release NE, weak positivity in the stroma may be extra-cellularly secreted protein. Examining a prostate cancer expression dataset generated by Taylor et al (37), we observed strong positive correlation between *CD33* and *ELANE* (gene encoding NE) expression (Fig 7B). Examining the larger TCGA Provisional dataset, we similarly observed strong positive correlation between *CD33* and *ELANE* expression (Supplementary Fig 3A). Importantly, *CD33* expression in this dataset appeared to associate with clinical outcomes; high *CD33* expression predicted significantly reduced recurrence free survival (Fig 7C). High *CD33* expression was also significantly associated higher primary Gleason score (Supplementary Fig 3B). Therefore, we hypothesized that CD33 MDSCs, which expand locally and systemically in patients with prostate cancer and other malignancies, may produce NE within the tumor microenvironment. Accordingly, sequential prostate sections from an HG-PIN sample from a patient with prostate cancer revealed that CD33+ cells likewise stained for NE (Fig 7D). Double immunofluorescence for NE and CD33 in confirmed co-localization (Fig 7E), with staining both inside and outside of the nucleus (nuclei stained in blue). Moreover, immunofluorescence revealed foci of NE positivity within glandular prostatic epithelium, suggesting possible internalization of secreted NE within endosomes (Fig 7E, middle), consistent with *in-vitro* studies demonstrating that NE internalization by cancer cells leads to enhanced proliferation (11, 38).

Discussion

The tumor microenvironment strongly influences cancer development, progression, and dissemination; thus, better understanding of the complex interactions between tumor cells and surrounding reactive stroma shows promise of uncovering new therapies. Recent data indicate that myeloid-derived cells increase in number locally and systemically during cancer growth in mice and humans, and their expansion is associated with worse disease outcomes (25, 28). These cells are often termed myeloid-derived suppressor cells (MDSCs) due to their ability to suppress adaptive immune responses. However, in addition to their suppressor functions, MDSCs, particularly the granulocytic subtype, exert direct effects on tumor cells, enhancing proliferation, migration, and invasion (25, 28). Here we demonstrate that granulocytic MDSCs accumulate in PC3 prostate cancer xenografts and expand in peripheral blood as a function of tumor growth in athymic mice, in the absence of potential suppression of T-cell activation. MDSC depletion after tumors become established results in reduced xenograft growth, confirming an important role for these cells in tumor progression. Indeed, in a xenograft model using canine Ace-1 prostate cancer cells, MDSCs were similarly shown to facilitate tumor growth when co-injected with cancer cells into athymic mice (39). Although this study suggested a direct pro-tumorigenic role for MDSCs in the absence of adaptive immunity, the number of MDSCs co-injected was arbitrary and likely supraphysiological. Moreover, this study did not investigate the dynamics of MDSCs during tumor growth or whether depletion has a mitigating impact on tumor burden. Notably, inhibition of MDSC recruitment or MDSC depletion reduced tumor growth in *Pten*-null prostate cancer mouse models (26, 27, 29, 30). We confirm that granulocytic MDSCs infiltrate *Pten*-null prostate lesions and localize with proliferative cancer cells. Moreover, lesion infiltration is associated with increased peripheral circulation of MDSCs, recapitulating the phenomenon seen in human prostate cancer patients. Given these data, we believe that MDSC accumulation is a general response to tumorigenesis and not simply an effect of xenografting in an immunodeficient host. Indeed, MDSC accumulation and recruitment is known to be a tumor-induced phenomenon in response to cancer cell expression of cytokines and chemokines like IL-6, IL-8, CSF-1, G-CSF, and GM-CSF (24, 28). However, we acknowledge that we did not measure MDSC numbers in mock-injected mice or in mice injected with non-tumorogenic cells such as RWPE-1.

The attenuating effect of MDSC depletion on *Pten*-null prostate tumor growth is attributed to both improved T-cell function and direct promotion of proliferation and evasion of cellular senescence (26, 27, 29, 30). However, since these experiments were performed in immune-competent mice, the contribution of direct versus indirect effects of MDSCs cannot be distinguished. By performing MDSC depletion in athymic mice with human prostate cancer xenografts, we not only confirm the importance of MDSCs in promoting tumor progression with two different human prostate cancer cell lines, we demonstrate that some MDSC-mediated effects are independent of T-cell suppression – possibly due to direct tumor stimulation.

There are a number of ways that MDSCs can promote cancer cell proliferation, migration, and invasion, including secretion of growth factors, pro-angiogenic factors, and proteases. Indeed, transcriptomic analyses of MDSCs reveal enrichment for proteases like MMP-9 and

NE (31, 32). While MDSC-derived MMP9 is known to mediate growth, angiogenesis, and metastasis of many cancers, the role of MDSC-derived NE remains unclear (40). Moreover, NE in prostate cancer specifically has not been investigated, despite reports showing that lesion infiltration and peripheral expansion of granulocytic cells correlates with worse patient outcomes (6, 29). Here we demonstrate that NE is active in prostate cancer xenografts in athymic mice, and its activity is elevated in *Pten*-null prostates compared to controls. While its name implies a neutrophil source, NE is actually expressed by a variety of cell types, including immune cells (myeloid and lymphoid) and epithelial and mesenchymal cells like breast cancer and smooth muscle cells (41, 42). We find that only infiltrating cells, not prostate cancer cells, express NE, since *ELANE* mRNA was only detected with mouse specific primers in both PC3 and C4-2 xenografts. We propose that CD33+ MDSCs are an important source of NE within the human prostate cancer microenvironment, as *CD33* and *ELANE* mRNA expression are strongly correlated in human prostate cancer specimens, and immunohistochemistry and immunofluorescence suggests cellular co-localization.

The pro-tumor role of NE has been explored in both cancer mouse models and human cancer patients. NE protein and activity is significantly elevated in sera of lung and colon cancer patients compared to healthy individuals, and correlates with disease progression (13, 43). Furthermore, NE deletion in lung and breast cancer mouse models results in reduced numbers of tumors and smaller tumors, supporting a functional role in tumor development and progression (11, 12, 14). Here we demonstrate that NE activity promotes prostate cancer xenograft growth of PC3 and C4-2 cell lines, since the NE inhibitor sivelestat exerts tumor inhibitory effects. We anticipate that NE inhibition would bear similar results in the *Pten*-null prostate cancer model, and detailed pharmacologic and genetic studies are planned to directly address this question.

While the efficacy of sivelestat in inhibiting primary growth of colon cancer xenografts in athymic mice was recently reported (13), the mechanism of action was not directly linked to NE inhibition. Here we find that sivelestat functions by directly impeding NE-induced effects. NE may induce cancer cell proliferation via several mechanisms, such as internalization of NE leading to degradation of IRS-1 or transactivation of cell surface receptors such as EGFR and TLR4 (11, 12, 18). We find that NE activates MAPK signaling in prostate cancer cells, which is dependent on enzymatic activity. Given its rapid actions, we suspect that NE-induced MAPK activation is likely due to transactivation of receptor tyrosine kinases, although further analysis will be necessary to elucidate specific receptors involved. NE-induced MAPK signaling is also functionally significant, leading to downstream ERK-dependent gene transcription and proliferation. Moreover, NE stimulates migration and invasion, both of which are essential for the development of metastases. Accordingly, both genetic deletion and pharmacologic inhibition of NE consistently results in decreased metastasis formation *in-vivo* (20).

The pro-metastatic role of NE in mouse models has partially been attributed to its involvement in neutrophil extracellular trap (NET) formation, or NETosis. NE is not only an essential mediator of NETosis, required for enzymatic histone degradation and chromatin decondensation prior to NET extrusion, but is also an integral component of fully formed

NETs (19, 20). Therefore, NE may be localized to several different compartments – intracellular (granular, and even nuclear) or extracellular, consistent with the staining seen in Fig 7 and Supplementary Fig 2. Cancer cells secrete factors that predispose granulocytes to undergo NETosis, leading to enhanced primary tumor growth, metastatic initiation and colonization, and cancer-associated morbidities like thrombosis and end organ damage (21–23). Indeed, prostate cancer patients have elevated plasma concentrations of G-CSF and IL8, two factors that likely prime circulating and infiltrating granulocytic MDSCs for NETosis (24, 27). It is possible that our observed reduction of prostate cancer xenograft growth with the NE inhibitor sivelestat is partially due to NETosis impairment *in-vivo*. However, the ability of NE alone to promote proliferation, migration, and invasion of prostate cancer cells suggests a discrete role in regulating tumor progression.

Intriguingly, endogenous NE inhibitors, like SERPINB1 and elafin, are ubiquitously expressed, and their down-regulation in cancer cells is associated with aggressive phenotypes (12, 44, 45). In addition to protease inhibitory functions, these proteins are important in anti-microbial, anti-inflammatory, and apoptotic pathways, and in fact can diminish NET formation (46, 47). *SERPINB1* expression particularly is down-regulated early in the development of prostatic intraepithelial neoplasia (PIN) and remains low in prostate cancer as compared to normal epithelium (48, 49). This expression pattern is also apparent at the protein level, since down-regulation of SERPINB1 in prostate cancer was recently shown using a proteomic approach (50). Given these observations, along with our results, it is tempting to postulate that down-regulation of SERPINB1 within prostatic epithelium during PIN and cancer formation might permit NE to exert proliferative, migratory, and invasive effects.

In summary, our findings demonstrate that granulocytic MDSCs directly contribute to prostate cancer xenograft growth in athymic mice, in the absence of suppressive effects on T-cell function. Intra-tumoral NE may provide a novel mechanistic and potentially targetable link between MDSC infiltration and prostate cancer progression.

Supplementary Material

Refer to Web version on PubMed Central for supplementary material.

Acknowledgments

Financial Support: S.R. Hammes received NIHR01GM101709, I. Lerman received NIHF30CA203517, J.J. Krolewski received NIHR01CA151753, J.J. Krolewski and K.L. Nastiuk received NIHP30CA016056, K.L. Nastiuk received HHS-6-15SF from the S.A.S. Foundation

References

1. Strasner A, Karin M. Immune Infiltration and Prostate Cancer. Frontiers in oncology. 2015; 5:128. [PubMed: 26217583]
2. Gurel B, Lucia MS, Thompson IM Jr, Goodman PJ, Tangen CM, Kristal AR, et al. Chronic inflammation in benign prostate tissue is associated with high-grade prostate cancer in the placebo arm of the prostate cancer prevention trial. Cancer epidemiology, biomarkers & prevention : a publication of the American Association for Cancer Research, cosponsored by the American Society of Preventive Oncology. 2014; 23(5):847–56.

3. Sharma J, Gray KP, Harshman LC, Evan C, Nakabayashi M, Fichorova R, et al. Elevated IL-8, TNF-alpha, and MCP-1 in men with metastatic prostate cancer starting androgen-deprivation therapy (ADT) are associated with shorter time to castration-resistance and overall survival. The Prostate. 2014; 74(8):820–8. [PubMed: 24668612]
4. Chi N, Tan Z, Ma K, Bao L, Yun Z. Increased circulating myeloid-derived suppressor cells correlate with cancer stages, interleukin-8 and −6 in prostate cancer. International journal of clinical and experimental medicine. 2014; 7(10):3181–92. [PubMed: 25419348]
5. Shafique K, Proctor MJ, McMillan DC, Qureshi K, Leung H, Morrison DS. Systemic inflammation and survival of patients with prostate cancer: evidence from the Glasgow Inflammation Outcome Study. Prostate cancer and prostatic diseases. 2012; 15(2):195–201. [PubMed: 22343838]
6. Tang L, Li X, Wang B, Luo G, Gu L, Chen L, et al. Prognostic Value of Neutrophil-to-Lymphocyte Ratio in Localized and Advanced Prostate Cancer: A Systematic Review and Meta-Analysis. PloS one. 2016; 11(4):e0153981. [PubMed: 27096158]
7. Lorente D, Mateo J, Templeton AJ, Zafeiriou Z, Bianchini D, Ferraldeschi R, et al. Baseline neutrophil-lymphocyte ratio (NLR) is associated with survival and response to treatment with second-line chemotherapy for advanced prostate cancer independent of baseline steroid use. Ann Oncol. 2015; 26(4):750–5. [PubMed: 25538172]
8. Gentles AJ, Newman AM, Liu CL, Bratman SV, Feng W, Kim D, et al. The prognostic landscape of genes and infiltrating immune cells across human cancers. Nature medicine. 2015; 21(8):938–45.
9. Komatsu N, Matsueda S, Tashiro K, Ioji T, Shichijo S, Noguchi M, et al. Gene expression profiles in peripheral blood as a biomarker in cancer patients receiving peptide vaccination. Cancer. 2012; 118(12):3208–21. [PubMed: 22071976]
10. Araki H, Pang X, Komatsu N, Soejima M, Miyata N, Takaki M, et al. Haptoglobin promoter polymorphism rs5472 as a prognostic biomarker for peptide vaccine efficacy in castration-resistant prostate cancer patients. Cancer immunology, immunotherapy : CII. 2015; 64(12):1565–73. [PubMed: 26428930]
11. Houghton AM, Rzymkiewicz DM, Ji H, Gregory AD, Egea EE, Metz HE, et al. Neutrophil elastase-mediated degradation of IRS-1 accelerates lung tumor growth. Nature medicine. 2010; 16(2):219–23.
12. Caruso JA, Akli S, Pageon L, Hunt KK, Keyomarsi K. The serine protease inhibitor elafin maintains normal growth control by opposing the mitogenic effects of neutrophil elastase. Oncogene. 2014
13. Ho AS, Chen CH, Cheng CC, Wang CC, Lin HC, Luo TY, et al. Neutrophil elastase as a diagnostic marker and therapeutic target in colorectal cancers. Oncotarget. 2014; 5(2):473–80. [PubMed: 24457622]
14. Gong L, Cumpian AM, Caetano MS, Ochoa CE, De la Garza MM, Lapid DJ, et al. Promoting effect of neutrophils on lung tumorigenesis is mediated by CXCR2 and neutrophil elastase. Molecular cancer. 2013; 12(1):154. [PubMed: 24321240]
15. Pivetta E, Danussi C, Wassermann B, Modica TM, Del Bel Belluz L, Canzonieri V, et al. Neutrophil elastase-dependent cleavage compromises the tumor suppressor role of EMILIN1. Matrix biology : journal of the International Society for Matrix Biology. 2014; 34:22–32. [PubMed: 24513040]
16. El Rayes T, Catena R, Lee S, Stawowczyk M, Joshi N, Fischbach C, et al. Lung inflammation promotes metastasis through neutrophil protease-mediated degradation of Tsp-1. Proceedings of the National Academy of Sciences of the United States of America. 2015; 112(52):16000–5. [PubMed: 26668367]
17. Grosse-Steffen T, Giese T, Giese N, Longerich T, Schirmacher P, Hansch GM, et al. Epithelial-to-mesenchymal transition in pancreatic ductal adenocarcinoma and pancreatic tumor cell lines: the role of neutrophils and neutrophil-derived elastase. Clinical & developmental immunology. 2012; 2012:720768. [PubMed: 23227088]
18. Wada Y, Yoshida K, Tsutani Y, Shigematsu H, Oeda M, Sanada Y, et al. Neutrophil elastase induces cell proliferation and migration by the release of TGF-alpha, PDGF and VEGF in esophageal cell lines. Oncology reports. 2007; 17(1):161–7. [PubMed: 17143494]

19. Papayannopoulos V, Metzler KD, Hakkim A, Zychlinsky A. Neutrophil elastase and myeloperoxidase regulate the formation of neutrophil extracellular traps. The Journal of cell biology. 2010; 191(3):677–91. [PubMed: 20974816]
20. Cools-Lartigue J, Spicer J, Najmeh S, Ferri L. Neutrophil extracellular traps in cancer progression. Cellular and molecular life sciences : CMLS. 2014; 71(21):4179–94. [PubMed: 25070012]
21. Cedervall J, Zhang Y, Huang H, Zhang L, Femel J, Dimberg A, et al. Neutrophil Extracellular Traps Accumulate in Peripheral Blood Vessels and Compromise Organ Function in Tumor-Bearing Animals. Cancer research. 2015; 75(13):2653–62. [PubMed: 26071254]
22. Cools-Lartigue J, Spicer J, McDonald B, Gowing S, Chow S, Giannias B, et al. Neutrophil extracellular traps sequester circulating tumor cells and promote metastasis. The Journal of clinical investigation. 2013
23. Demers M, Wong SL, Martinod K, Gallant M, Cabral JE, Wang Y, et al. Priming of neutrophils toward NETosis promotes tumor growth. Oncoimmunology. 2016; 5(5):e1134073. [PubMed: 27467952]
24. Alfaro C, Teijeira A, Onate C, Perez G, Sanmamed MF, Andueza MP, et al. Tumor-Produced Interleukin-8 Attracts Human Myeloid-Derived Suppressor Cells and Elicits Extrusion of Neutrophil Extracellular Traps (NETs). Clinical cancer research : an official journal of the American Association for Cancer Research. 2016; 22(15):3924–36. [PubMed: 26957562]
25. Coffelt SB, Wellenstein MD, de Visser KE. Neutrophils in cancer: neutral no more. Nature reviews Cancer. 2016; 16(7):431–46. [PubMed: 27282249]
26. Wang G, Lu X, Dey P, Deng P, Wu CC, Jiang S, et al. Targeting YAP-Dependent MDSC Infiltration Impairs Tumor Progression. Cancer discovery. 2016; 6(1):80–95. [PubMed: 26701088]
27. Hossain DM, Pal SK, Moreira D, Duttagupta P, Zhang Q, Won H, et al. TLR9-Targeted STAT3 Silencing Abrogates Immunosuppressive Activity of Myeloid-Derived Suppressor Cells from Prostate Cancer Patients. Clinical cancer research : an official journal of the American Association for Cancer Research. 2015; 21(16):3771–82. [PubMed: 25967142]
28. Marvel D, Gabrilovich DI. Myeloid-derived suppressor cells in the tumor microenvironment: expect the unexpected. The Journal of clinical investigation. 2015; 125(9):3356–64. [PubMed: 26168215]
29. Di Mitri D, Toso A, Chen JJ, Sarti M, Pinton S, Jost TR, et al. Tumour-infiltrating Gr-1+ myeloid cells antagonize senescence in cancer. Nature. 2014; 515(7525):134–7. [PubMed: 25156255]
30. Garcia AJ, Ruscetti M, Arenzana TL, Tran LM, Bianci-Frias D, Sybert E, et al. Pten null prostate epithelium promotes localized myeloid-derived suppressor cell expansion and immune suppression during tumor initiation and progression. Molecular and cellular biology. 2014; 34(11):2017–28. [PubMed: 24662052]
31. Fridlender ZG, Sun J, Mishalian I, Singhal S, Cheng G, Kapoor V, et al. Transcriptomic analysis comparing tumor-associated neutrophils with granulocytic myeloid-derived suppressor cells and normal neutrophils. PloS one. 2012; 7(2):e31524. [PubMed: 22348096]
32. Youn JI, Collazo M, Shalova IN, Biswas SK, Gabrilovich DI. Characterization of the nature of granulocytic myeloid-derived suppressor cells in tumor-bearing mice. Journal of leukocyte biology. 2012; 91(1):167–81. [PubMed: 21954284]
33. Singh S, Agarwal M, Bhatt A, Goyal A, Moholkar VS. Ultrasound enhanced enzymatic hydrolysis of Parthenium hysterophorus: A mechanistic investigation. Bioresource technology. 2015; 192:636–45. [PubMed: 26094188]
34. Mitra S, Modi KD, Foster TH. Enzyme-activatable imaging probe reveals enhanced neutrophil elastase activity in tumors following photodynamic therapy. Journal of biomedical optics. 2013; 18(10):101314. [PubMed: 23897439]
35. Prizant H, Taya M, Lerman I, Light A, Sen A, Mitra S, et al. Estrogen maintains myometrial tumors in a lymphangioleiomyomatosis model. Endocrine-related cancer. 2016; 23(4):265–80. [PubMed: 26880751]
36. Sfanos KS, Wilson BA, De Marzo AM, Isaacs WB. Acute inflammatory proteins constitute the organic matrix of prostatic corpora amylacea and calculi in men with prostate cancer. Proceedings of the National Academy of Sciences of the United States of America. 2009; 106(9):3443–8. [PubMed: 19202053]

37. Taylor BS, Schultz N, Hieronymus H, Gopalan A, Xiao Y, Carver BS, et al. Integrative genomic profiling of human prostate cancer. Cancer cell. 2010; 18(1):11–22. [PubMed: 20579941]
38. Gregory AD, Hale P, Perlmutter DH, Houghton AM. Clathrin pit-mediated endocytosis of neutrophil elastase and cathepsin G by cancer cells. The Journal of biological chemistry. 2012; 287(42):35341–50. [PubMed: 22915586]
39. Park SI, Lee C, Sadler WD, Koh AJ, Jones J, Seo JW, et al. Parathyroid hormone-related protein drives a CD11b+Gr1+ cell-mediated positive feedback loop to support prostate cancer growth. Cancer research. 2013; 73(22):6574–83. [PubMed: 24072746]
40. Deryugina EI, Zajac E, Juncker-Jensen A, Kupriyanova TA, Welter L, Quigley JP. Tissue-infiltrating neutrophils constitute the major in vivo source of angiogenesis-inducing MMP-9 in the tumor microenvironment. Neoplasia. 2014; 16(10):771–88. [PubMed: 25379015]
41. Hunt KK, Wingate H, Yokota T, Liu Y, Mills GB, Zhang F, et al. Elafin, an inhibitor of elastase, is a prognostic indicator in breast cancer. Breast cancer research : BCR. 2013; 15(1):R3. [PubMed: 23320734]
42. Kim YM, Haghighat L, Spiekerkoetter E, Sawada H, Alvira CM, Wang L, et al. Neutrophil elastase is produced by pulmonary artery smooth muscle cells and is linked to neointimal lesions. The American journal of pathology. 2011; 179(3):1560–72. [PubMed: 21763677]
43. Vaguliene N, Zemaitis M, Lavinskiene S, Miliauskas S, Sakalauskas R. Local and systemic neutrophilic inflammation in patients with lung cancer and chronic obstructive pulmonary disease. BMC immunology. 2013; 14:36. [PubMed: 23919722]
44. Chou RH, Wen HC, Liang WG, Lin SC, Yuan HW, Wu CW, et al. Suppression of the invasion and migration of cancer cells by SERPINB family genes and their derived peptides. Oncology reports. 2012; 27(1):238–45. [PubMed: 21993616]
45. Willmes C, Kumar R, Becker JC, Fried I, Rachakonda PS, Poppe LM, et al. SERPINB1 expression is predictive for sensitivity and outcome of cisplatin-based chemotherapy in melanoma. Oncotarget. 2016; 7(9):10117–32. [PubMed: 26799424]
46. Heit C, Jackson BC, McAndrews M, Wright MW, Thompson DC, Silverman GA, et al. Update of the human and mouse SERPIN gene superfamily. Human genomics. 2013; 7:22. [PubMed: 24172014]
47. Farley K, Stolley JM, Zhao P, Cooley J, Remold-O'Donnell E. A serpinB1 regulatory mechanism is essential for restricting neutrophil extracellular trap generation. Journal of immunology. 2012; 189(9):4574–81.
48. Ashida S, Nakagawa H, Katagiri T, Furihata M, Iiizumi M, Anazawa Y, et al. Molecular features of the transition from prostatic intraepithelial neoplasia (PIN) to prostate cancer: genome-wide gene-expression profiles of prostate cancers and PINs. Cancer research. 2004; 64(17):5963–72. [PubMed: 15342375]
49. Altintas DM, Allioli N, Decaussin M, de Bernard S, Ruffion A, Samarut J, et al. Differentially expressed androgen-regulated genes in androgen-sensitive tissues reveal potential biomarkers of early prostate cancer. PloS one. 2013; 8(6):e66278. [PubMed: 23840433]
50. Davalieva K, Kostovska IM, Kiprijanovska S, Markoska K, Kubelka-Sabit K, Filipovski V, et al. Proteomics analysis of malignant and benign prostate tissue by 2D DIGE/MS reveals new insights into proteins involved in prostate cancer. The Prostate. 2015; 75(14):1586–600. [PubMed: 26074449]

Implications

This report suggests that MDSCs and NE are physiologically important mediators of prostate cancer progression, and may serve as potential biomarkers and therapeutic targets.

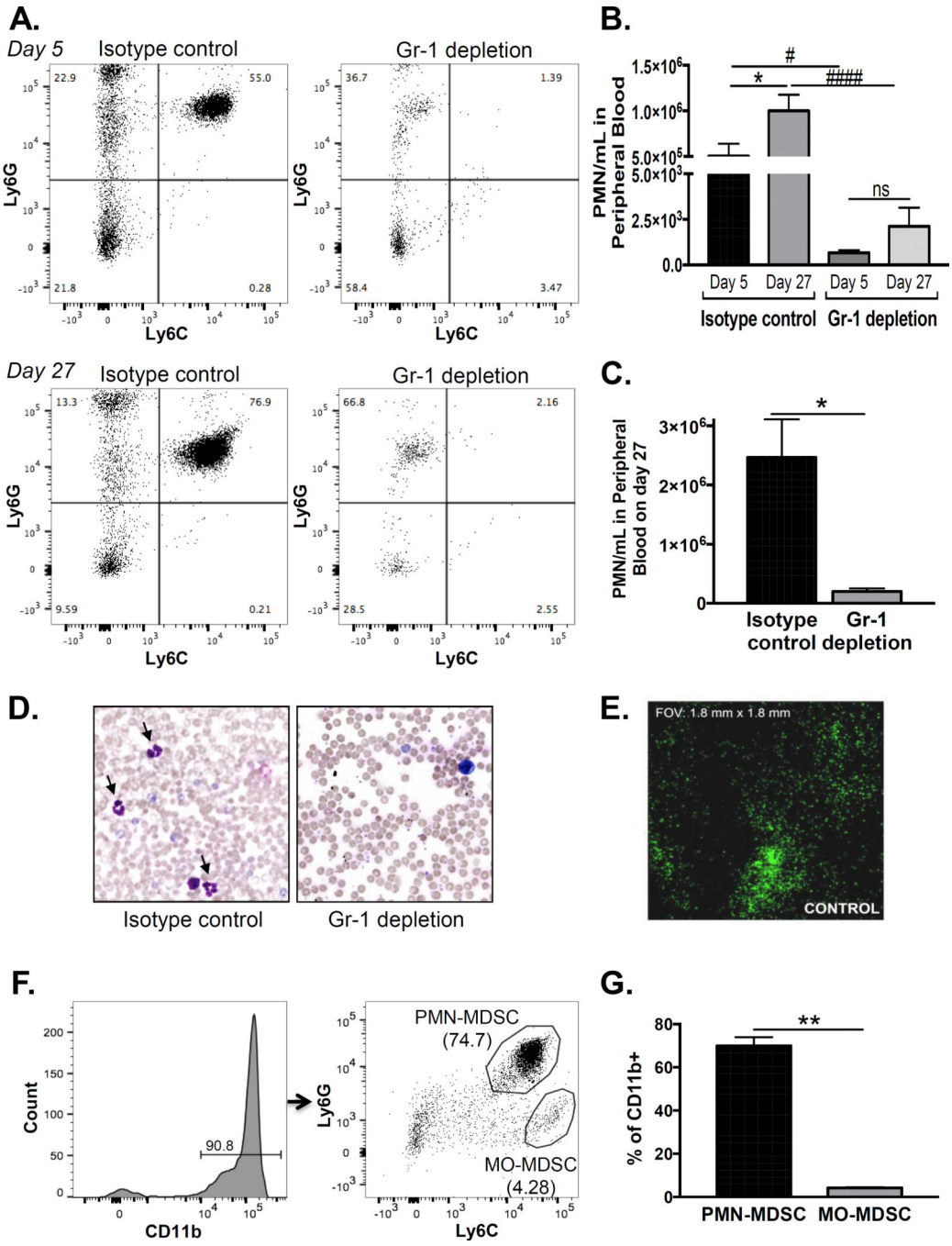

Figure 1. Granulocytic MDSCs expand in peripheral blood and infiltrate human prostate cancer xenografts

A. Peripheral blood MDSCs were assessed by flow cytometry in PC3 xenograft bearing nude mice on days 5 and 27 after initiation of isotype or Gr-1 antibody treatment. Representative plots of Ly6G vs. Ly6C expression, gated on CD11b+ myeloid cells, are shown (n=4/treatment group). B. The number of Ly6G+/Ly6C+ cells in Gr-1 depleted mice was compared to isotype controls on days 5 and 27 using one-way ANOVA with Bonferroni post-hoc testing (#compares day 5 numbers, $p < 0.05$, ####compares day 27 numbers, $p < 0.0001$). Isotype control and Gr-1 depletion groups on day 27 were compared to day 5 using

one-way ANOVA with Bonferroni post-hoc testing (*compares days 5 and 27 control, $p < 0.05$, ns = not significant between days 5 and 27 depletion). C. The number of peripheral blood granulocytes on day 27 by automated cell counting was compared between isotype control and Gr-1 depletion mice using unpaired two-tailed t-test (n=4/treatment group; *$p < 0.05$). D. Representative Wright-Giemsa stained peripheral blood smears of isotype control and Gr-1 depletion mice on day 27. Arrows are cells with polymorphonuclear morphology. E. Whole mount immunofluorescence for Gr-1 in an untreated PC3 xenograft. F. Tumor infiltrating MDSCs were assessed by flow cytometry in control PC3 xenografts. Representative plot of Ly6G vs. Ly6C expression, gated on the CD11b+ myeloid population, is shown. Granulocytic (PMN; $Ly6G^{High}/Ly6C^{High}$) and monocytic (MO; $Ly6G^{Low}/Ly6C^{High}$) populations are indicated. G. The number of granulocytic and monocytic MDSCs was compared using paired two-tailed t-test (n=3; **$p < 0.01$).

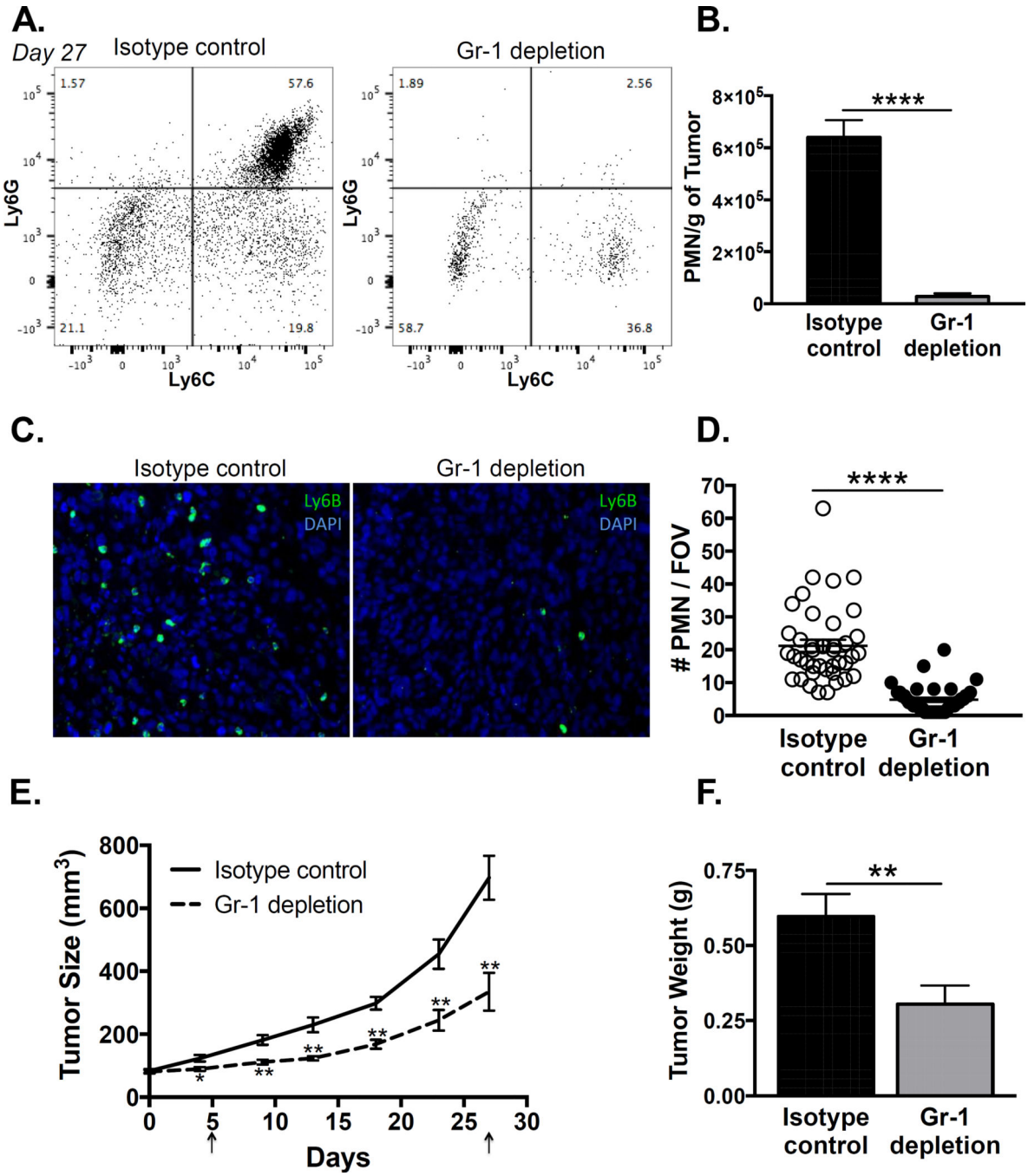

Figure 2. Depletion of MDSCs with Gr-1 antibody suppresses human prostate cancer xenograft growth

A. Tumor infiltrating MDSCs were assessed by flow cytometry in PC3 xenograft bearing nude mice on day 27 after initiation of isotype or Gr-1 antibody treatment. Representative plots of Ly6G versus Ly6C expression, gated on the CD11b+ myeloid population, are shown (n=8/treatment group). B. The number of infiltrating granulocytic MDSCs ($Ly6G^{High}$/ $Ly6C^{High}$) was compared between isotype control and Gr-1 depletion tumors, normalized to tumor weight, using unpaired two-tailed t-test (n=8; ****$p < 0.0001$). C. Representative immunofluorescence stain for Ly6B+ infiltrating granulocytic MDSCs in isotype control and

Gr-1 depletion tumors is shown. D. The number of Ly6B+ cells was compared between isotype control and Gr-1 depletion tumors using unpaired two-tailed t-test (n=40/treatment group, 5 fields of view/8 tumors; ****$p < 0.0001$). E. Tumor size (length × width^2 × 0.5) was measured every 3–4 days and compared between isotype control and Gr-1 depletion groups using unpaired two-tailed t-test (n=8 per treatment group; *$p < 0.05$, **$p<0.01$). Arrows indicate time points when MDSC depletion was assessed in peripheral blood. F. Tumor weight was compared between isotype control and Gr-1 depletion groups using unpaired two-tailed t-test (n=8 per treatment group; **$p=0.01$).

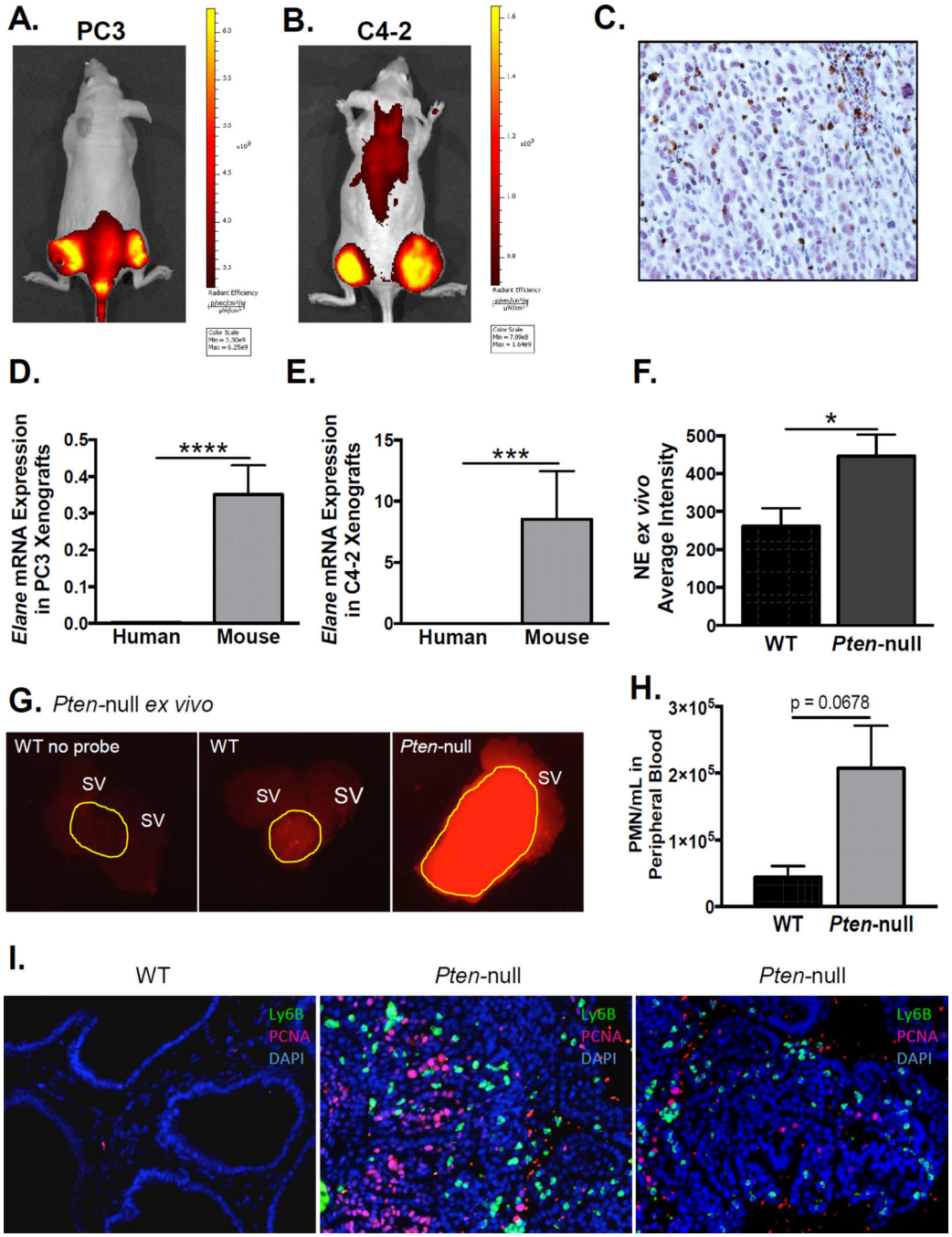

Figure 3. Infiltrating immune cells produce active neutrophil elastase in the prostate cancer microenvironment

Intra-tumoral neutrophil elastase activity was measured *in-vivo* using a NE specific optical probe in athymic nude mice bearing PC3 (A) and C4-2 (B) xenografts (n=3 per cell line). Representative IVIS images are shown. C. Immunohistochemistry of a representative PC3 xenograft using anti-NE antibody. Neutrophil elastase mRNA expression was quantified using quantitative PCR with human (*ELANE*) and mouse (*Elane*) specific primers for PC3 (D) and C4-2 (E) xenografts. Values were normalized to *GAPDH* and *Gapdh* mRNA expression, respectively. mRNA expression of mouse derived and human derived NE was

compared using paired Wilcoxon signed-rank test (n=23 for PC3 and n=12 for C4-2; ****p<0.0001, *** p<0.001). F. Intra-prostatic NE activity in the prostatic ROI was quantified using ImageJ and compared between *Pten*-null and WT mice using unpaired two-tailed t-test (n=4 for each genotype; *p<0.05). G. Intra-prostatic NE activity was measured *ex-vivo* following IV administration of a NE specific optical probe to *Pten*-null and wild-type (WT) mice. First panel from a WT mouse that received no probe. Yellow outline indicates prostatic region of interest. SV = seminal vesicle. H. Peripheral blood MDSCs were assessed using flow cytometry in *Pten*-null and wild-type (WT) mice. The number of Ly6G+/Ly6C+ cells was compared using unpaired two-tailed t-test (n = 3 for each genotype). I. Representative immunofluorescence stains for Ly6B+ infiltrating granulocytic MDSCs and PCNA positive proliferating epithelium in WT and two different *Pten*-null prostates is shown (n=3 total for each group).

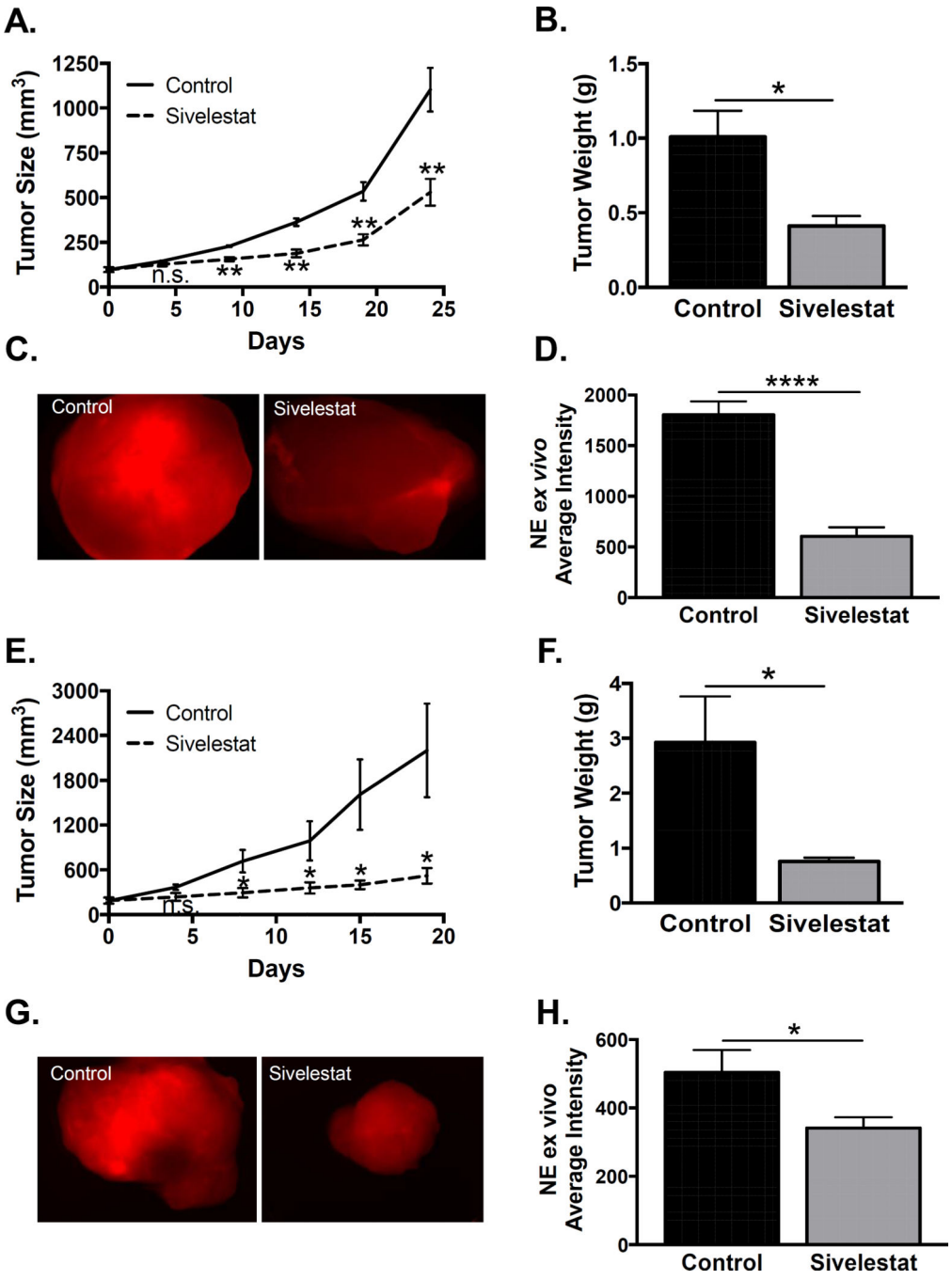

Figure 4. Inhibition of neutrophil elastase activity suppresses human prostate cancer xenograft growth

A. PC3 tumor size (length × width^2 × 0.5) was measured every 3–4 days and compared between vehicle control and sivelestat groups using unpaired two-tailed t-test. B. PC3 tumor weight was compared between vehicle control and sivelestat groups using unpaired two-tailed t-test (n=4 per treatment group; *p<0.05, **p<0.01). C. PC3 intra-tumoral neutrophil elastase activity was measured *ex-vivo* using an NE specific optical probe. D. PC3 intra-tumoral NE activity was quantified using ImageJ and compared between vehicle control and sivelestat groups using unpaired two-tailed t-test (n=8 for vehicle control, n=6 for sivelestat;

****p<0.0001). E. C4-2 tumor size was measured every 3–4 days and compared between vehicle control and sivelestat groups using unpaired two-tailed t-test. F. C4-2 tumor weight was compared between vehicle control and sivelestat groups using unpaired two-tailed t-test (n=5 for control, n=6 for sivelestat; *p<0.05). G. C4-2 intra-tumoral neutrophil elastase activity was measured *ex-vivo* using an NE specific optical probe. H. C4-2 intra-tumoral NE activity was quantified using ImageJ and compared between vehicle control and sivelestat groups using unpaired two-tailed t-test (n=7 for vehicle control, n=7 for sivelestat; *p<0.05).

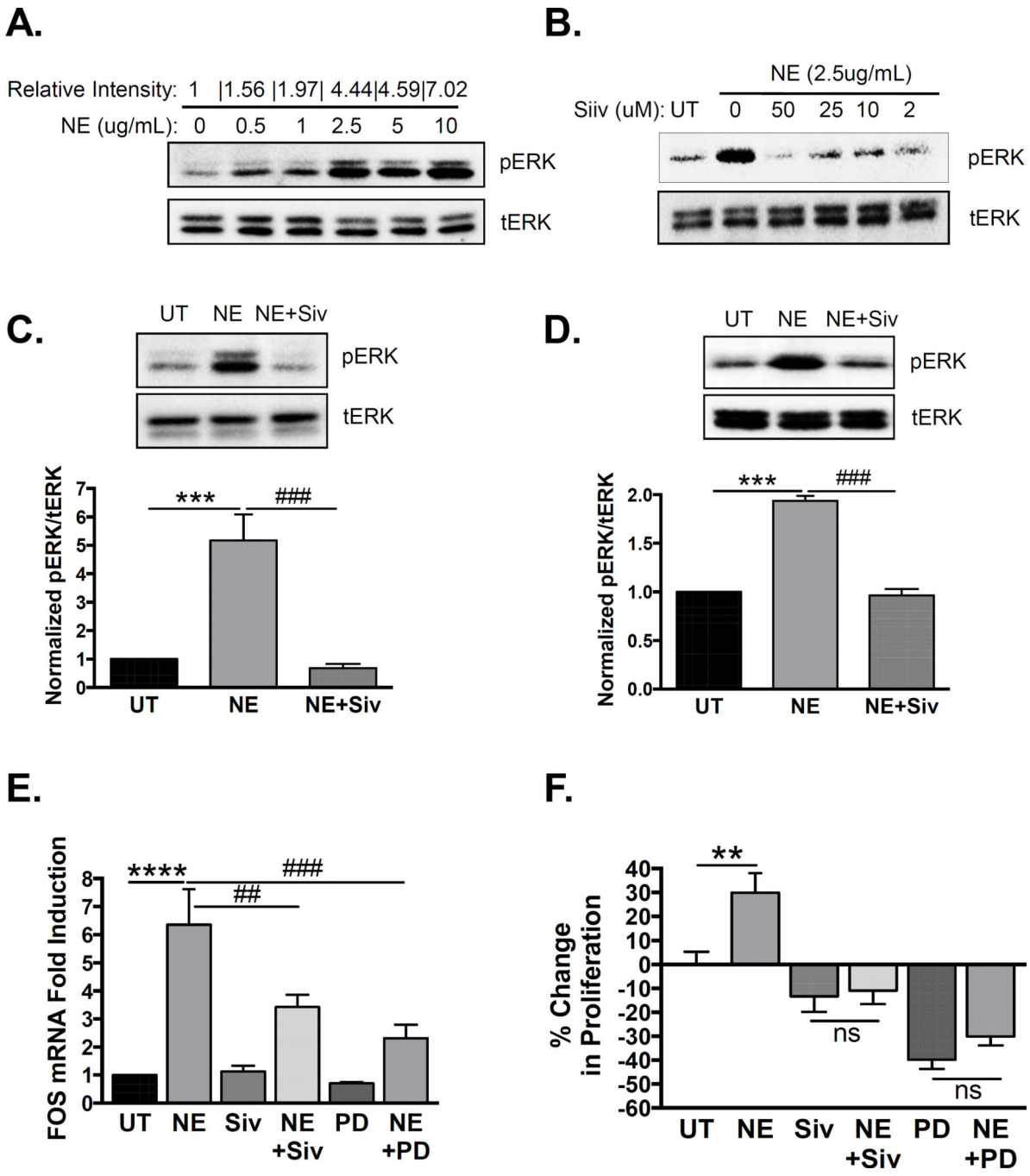

Figure 5. Neutrophil elastase activates MAPK signaling and induces MAPK-dependent gene transcription and proliferation in human prostate cancer cells

A. PC3 cells were serum starved and treated with increasing concentrations of NE for 15 minutes. pERK1/2 and tERK1/2 levels were examined by Western blot. Band densitometry of pERK1/2 to tERK1/2 was performed using ImageJ and normalized to untreated (0). B. PC3 cells were serum starved and treated with NE (2.5μg/mL) for 15 minutes in the presence of increasing concentrations of sivelestat. pERK1/2 and tERK1/2 levels were examined by Western blot. PC3 (C) or C4-2 (D) cells were serum starved and treated with NE (2.5μg/mL) for 15 minutes in the presence of sivelestat (2μM) or vehicle. pERK1/2 and

tERK1/2 levels were examined by Western blot, and band densitometry performed using ImageJ and normalized to untreated (UT) samples. Multiple comparisons were performed using row matched one-way ANOVA with Dunnett's post-hoc testing (n=6 for PC3 and n=3 for C4-2; ***p<0.001, ###p<0.001). E. C4-2 cells were serum starved and treated with NE (2.5μg/mL) for 6 hours in the presence of sivelestat (2μM), PD0325901 (50nM), or vehicle. *cFOS* mRNA expression was determined using quantitative PCR and normalized to *GAPDH*. Data were normalized to untreated samples and multiple comparisons were performed using row matched one-way ANOVA with Dunnett's post-hoc testing (n=4; ****p<0.0001, ##p<0.01, ###p<0.001). F. C4-2 cells were serum starved and treated with NE (2.5μg/mL) for 24 hours in the presence of sivelestat (2μM), PD0325901 (50nM), or vehicle. Proliferation was examined by BrdU incorporation, and data were plotted as percent change in proliferation relative to untreated samples. Multiple comparisons were performed using ordinary one-way ANOVA with Bonferroni's post-hoc testing (n=9; **p<0.01, ns=not significant).

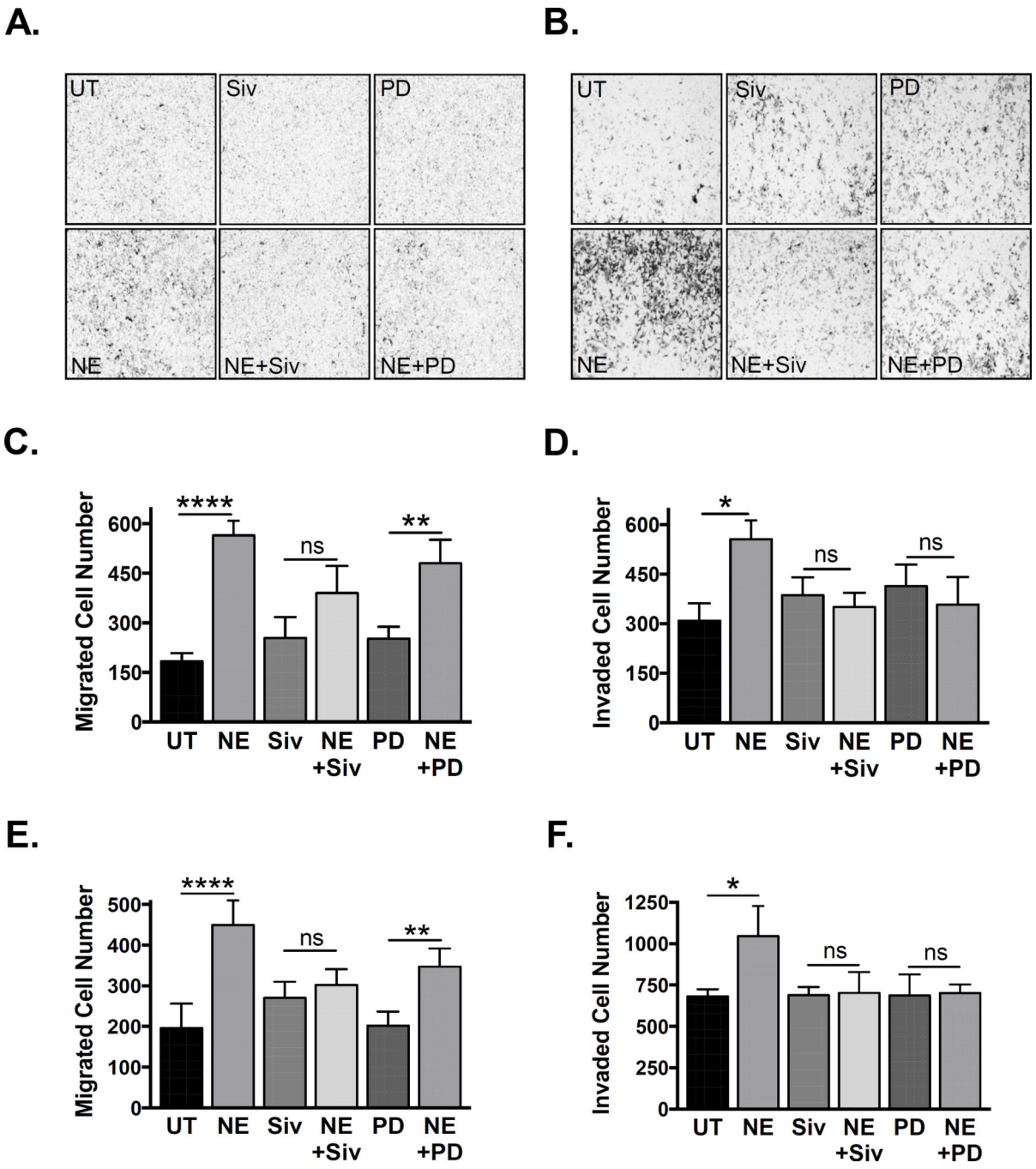

Figure 6. Neutrophil elastase induces migration and invasion in human prostate cancer cells

A. C4-2 cells were serum starved and transferred into the upper chambers of 8um uncoated transwells in the presence of NE (2.5 ug/mL), sivelestat (2 uM), PD0325901 (50 nM), or vehicle. Cells were allowed to migrate for 24 hours towards a chemotactic gradient of 10% FBS. B. C4-2 cells were serum starved and transferred into the upper chambers of 8um Matrigel coated transwells in the presence of NE (2.5 ug/mL), sivelestat (2 uM), PD0325901 (50 nM), or vehicle. Cells were allowed to invade for 24 hours towards a chemotactic gradient of 10% FBS. C. Number of migrated C4-2 cells was quantified using ImageJ.

Multiple comparisons were performed using row matched one-way ANOVA with Bonferroni's post-hoc testing (n = 4; **** $p < 0.0001$, ** $p < 0.01$, ns = not significant). D. Number of invaded C4-2 cells was quantified using ImageJ (n = 4; * $p < 0.05$, ns = not significant). E. Number of migrated PC3 cells was quantified using ImageJ (n = 3; **** $p < 0.0001$, ** $p < 0.01$, ns = not significant). F. Number of invaded PC3 cells was quantified using ImageJ (n = 3; * $p < 0.05$, ns = not significant).

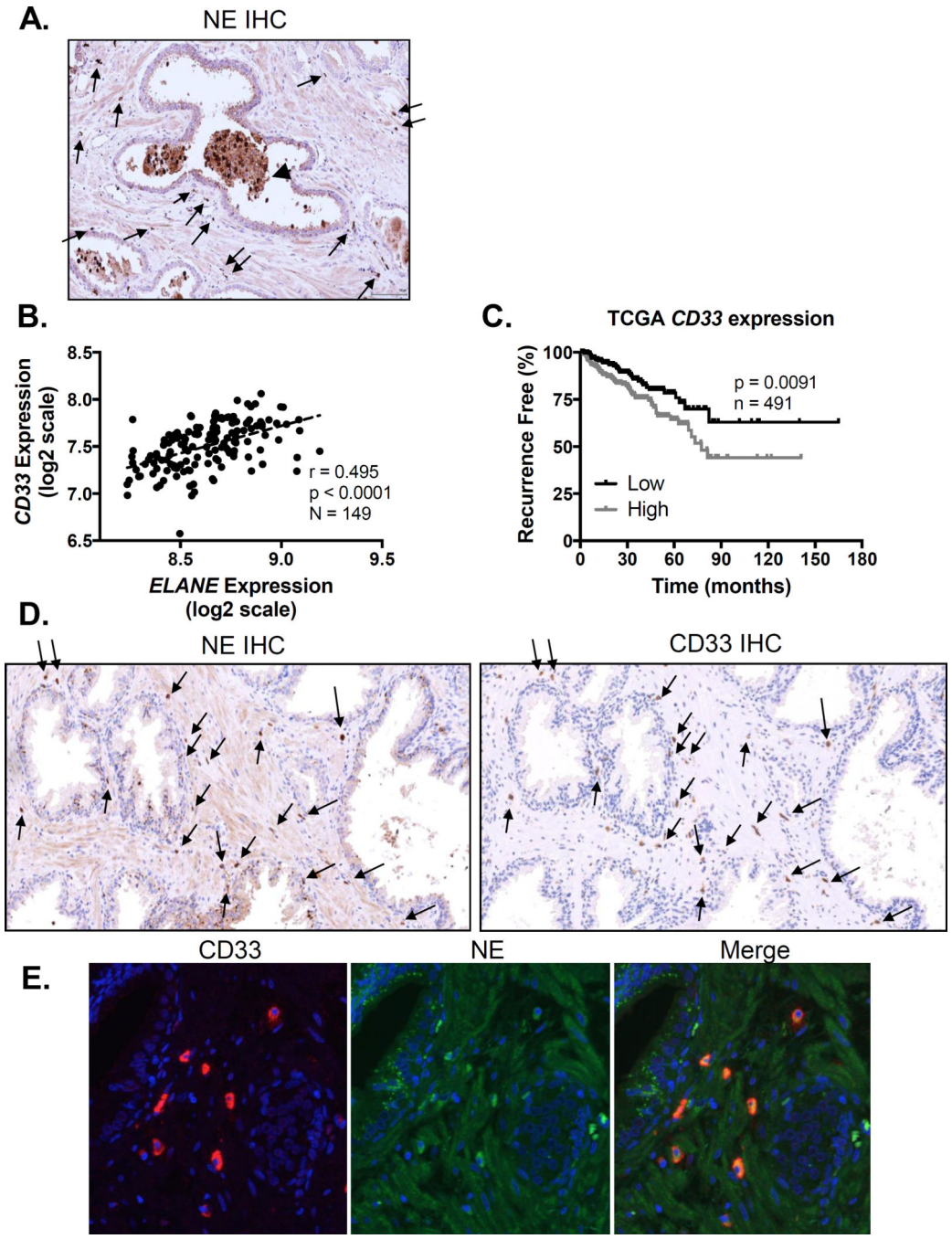

Figure 7. Neutrophil elastase is co-expressed with infiltrating CD33+ MDSCs in human prostates

A. Neutrophil elastase protein expression was determined by immunohistochemistry on human prostate cancer microarrays (image representative of n = 3 patients). Arrows indicate infiltrating NE positive cells. Arrowhead indicates NE positive glandular deposits. B. Human prostate cancer *CD33* and *ELANE* mRNA expression data were obtained from Taylor (37) and plotted to examine correlation using two-tailed Pearson correlation analysis. C. Kaplan-Meier plots for patients expressing CD33 above (high) and below (low) the median *CD33* expression threshold from the TCGA Provisional prostate cancer dataset

(downloaded from http://cancergenome.nih.gov/) were constructed. Differences in recurrence free survival were assessed using the log-rank (Mantel-Cox) test. D. NE and CD33 protein expression were determined by immunohistochemistry on consecutive human prostate cancer samples (images representative of n = 3 patients). Arrows indicate infiltrating cells double positive for NE and CD33. E. NE and CD33 protein co-localization in human prostates was confirmed by immunofluorescence.